

Varformer: Adapting VAR’s Generative Prior for Image Restoration

Siyang Wang, Feng Zhao

University of Science and Technology of China

siyangw@mail.ustc.edu.cn, fzhao956@ustc.edu.cn

Abstract

Generative models trained on extensive high-quality datasets effectively capture the structural and statistical properties of clean images, rendering them powerful priors for transforming degraded features into clean ones in image restoration. VAR, a novel image generative paradigm, surpasses diffusion models in generation quality by applying a next-scale prediction approach. It progressively captures both global structures and fine-grained details through the autoregressive process, consistent with the multi-scale restoration principle widely acknowledged in the restoration community. Furthermore, we observe that during the image reconstruction process utilizing VAR, scale predictions automatically modulate the input, facilitating the alignment of representations at subsequent scales with the distribution of clean images. To harness VAR’s adaptive distribution alignment capability in image restoration tasks, we formulate the multi-scale latent representations within VAR as the restoration prior, thus advancing our delicately designed VarFormer framework. The strategic application of these priors enables our VarFormer to achieve remarkable generalization on unseen tasks while also reducing training computational costs. Extensive experiments underscores that our VarFormer outperforms existing multi-task image restoration methods across various restoration tasks. The code is available at <https://github.com/siywang541/Varformer>.

1. Introduction

Image restoration (IR) aims to reconstruct a high-quality (HQ) image from its degraded low-quality (LQ) counterpart, making it widely applicable in various real-world scenarios, including photo processing, autonomous driving, and surveillance. Recent advances in deep learning have led to powerful IR approaches that excel at addressing specific types of degradation, such as denoising [47, 61, 62], deblurring [37, 38, 40], and low-light enhancement [12, 49, 50], etc. However, these task-specific models struggle with the varied and unpredictable degradations commonly present in

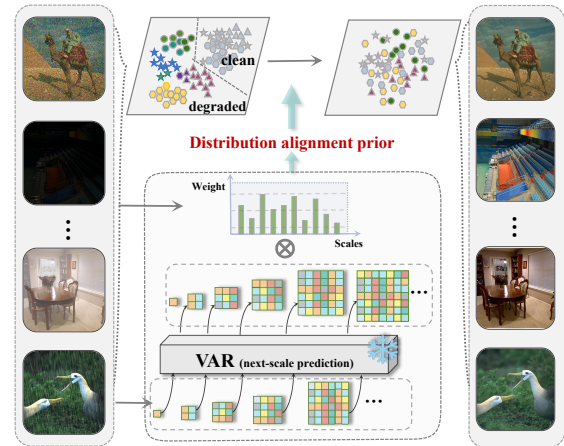


Figure 1. Motivation of VarFormer. (1) As the autoregressive scale evolves, VAR’s multi-scale representations shift focus from capturing global patterns at lower scales to highlighting fine-grained details at higher scales. (2) VAR’s scale predictions adaptively modulate the input to align with the distribution of clean images. Utilizing VAR’s alignment prior on varied scale features related to degradation types allows us to eliminate associated degradations.

real-world scenarios, emphasizing the need for a generalist approach capable of restoring multiple types of degradation.

Recently, several pioneers have sought to develop a universal image restoration model, making considerable strides in the field. MPRNet [55] designs a multi-stage architecture that progressively learns image restoration functions for various known degradations. AirNet [21] distinguishes various image degradation in latent space through a contrastive-based degraded encoder. IDR [60] adopts an ingredients-oriented paradigm to investigate the correlation among various restoration tasks. However, given the infinite possible solutions for each degraded image, relying exclusively on the degraded image as the sole feature source while neglecting the prior distribution of clean images represents a major limitation for these models in terms of structural reconstruction and realistic texture restoration.

To alleviate these limitations, some studies have focused on the impact of generative priors within the image restora-

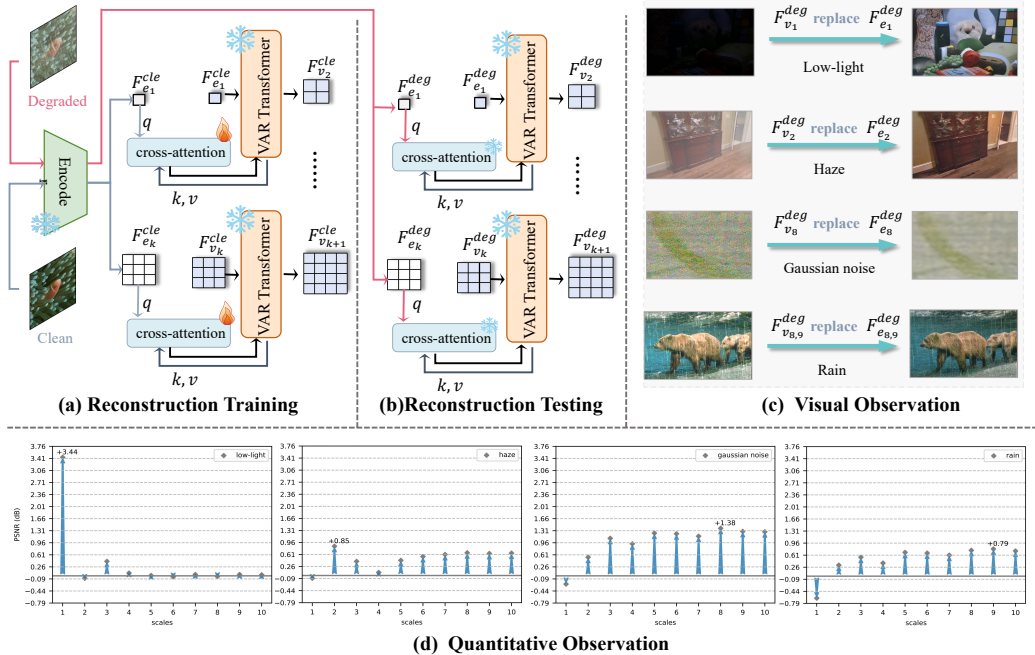


Figure 2. Illustration of our investigation about the multi-scale distribution alignment priors within VAR. (a) Reconstruction Training: To ensure the coherence of teacher-forcing-based autoregressive predictions, we employ cross-attention to inject multi-scale embeddings F_e obtained from the VQVAE encoder into the scale autoregression Transformer in VAR [39] for image reconstruction pre-training. During this process, we freeze the VAR and train only the cross-attention mechanism using clean images. (b) Reconstruction Testing: We feed degraded images into the trained VAR to obtain outputs from the VQVAE encoder, denoted as F_e^{deg} , and the multi-scale predictions from the VAR Transformer, denoted as F_v^{deg} . (c-d) Observation: By partially replacing F_e^{deg} with F_v^{deg} and mapping the modified multi-scale features back to the pixel space through the decoder, the disappearance of various degradations occurs when replacing different scale features, demonstrating a transition from capturing global information at lower scales to focusing on fine-grained details at higher scales.

tion (IR) community. These investigations are grounded in the characteristic that generative models inherently learn high-quality image reconstruction, enabling them to maintain robust high-quality priors that facilitate the transition of degraded features to the clean domain. These approaches perform IR tasks using the generative prior [18, 25, 45] from the GAN or diffusion models, achieving superior performance and demonstrating the effectiveness of generative prior for IR tasks. Recently, a novel generative paradigm, VAR, stands out in the image generation community, recognized for its efficiency and generation capabilities that surpass those of Stable Diffusion [39]. VAR generates images with progressively increasing resolutions by utilizing marker mapping for next-scale predictions, resolving the conflict between the inherent bidirectional and two-dimensional structural correlations in image patch labeling and the unidirectional nature of the autoregressive model.

Motivated by the powerful generative capabilities of VAR and the alignment between its endogenous scale representation and the widely recognized multi-scale restoration principle, we aim to explore the rich prior knowledge embedded in the pre-trained VAR across the scale dimen-

sion for restoration tasks. Our investigation reveals the adaptability of the autoregressive scale representation, as the VAR feature representation shifts from capturing wide-ranging global patterns at lower scales to highlighting intricate details at higher scales. As described in Fig. 2 a and b, we apply pre-trained VAR to reconstruct the paired clean and degraded images, respectively. When we replace the partially scale features of the degraded images obtained from the VQVAE encoder with the autoregressive generated scale features, the degradation of the images gradually diminishes. Specifically, Fig. 2 c shows that substituting lower scales can alleviate global degradations (e.g., low light and haze), while higher scales address local degradations (e.g., noise and rain). For a boarder investigation, we further perform a statistical analysis of the prior knowledge related to high-quality images, utilizing 100 paired images for each type of degradation. As illustrated in Fig. 3, VAR’s next-scale prediction projects the multi-scale latent representations of both degraded and clean images into a common space, thereby reducing the distribution gap between various degradations and clean images, demonstrating the model’s adaptive distribution alignment capability.

Building on the above observation, we develop a novel framework, named VarFormer, which integrates multi-scale distribution alignment priors from VAR to restore various degradation types within a single model. Specifically, to adaptively incorporate the valuable VAR scale priors associated with specific degradation types, we design the Degradation-Aware Enhancement (DAE) module that distinguishes different degradation types and filters out unnecessary interference, thereby providing effective guidance for the restoration process. Then, to alleviate structural warping and textural distortion resulting from the fusion of high-quality priors and low-quality degraded features, we present the Adaptive Feature Transformation (AFT) module. Furthermore, we employ an adaptive mixing strategy to effectively incorporate low-level features from the encoder, enhancing image details while mitigating potential information loss incurred by downsampling operations. By integrating these designs, our VarFormer not only captures a high-quality feature distribution that enables exceptional generalization on unseen tasks but also accelerates convergence, thus reducing training computational costs.

Our contributions are summarized as follows:

- We investigate the multi-scale representations of VAR and reveal its endogenous multi-scale distribution alignment priors, which transition from capturing global color information to focusing on fine-grained details, adaptively aligning the input images with clean images scale by scale as the autoregressive scale evolves.
- We propose the VarFormer framework integrated with multi-scale priors for multiple degradation restoration, embracing generalization capability on unseen tasks. To the best of our knowledge, this is the first attempt to explore generative priors from VAR for image restoration.
- Extensive experiments on six image restoration tasks demonstrate the efficiency and effectiveness of VarFormer, including deraining, deblurring, dehazing, low-light image enhancement, Gaussian and real denoising.

2. Related Work

2.1. Image Restoration

The purpose of image restoration is to reconstruct high quality natural images from the degraded images (e.g. noise, blur, rain drops). Early methods typically focus on incorporating various natural image priors along with hand-crafted features for specific degradation removal tasks [4, 13]. Recently, deep learning based methods have made compelling progress on various image restoration tasks. For instance, DGUNet is proposed based on Proximal Gradient Descent (PGD) algorithm for a gradient estimation strategy without loss of interpretability [34]. IDR [60] employs an ingredients-oriented paradigm to investigate the correlation among various restoration tasks. TransWeather [42] designs

a transformer-based network with learnable weather type queries to tackle various weather degradation.

2.2. Generative Priors in Image Restoration

The generative models trained on clean data excel at capturing the inherent structures of the image, enabling the generation of images that follow natural image distribution, which helps boost the performance in many low-level vision tasks. Generative Priors of pretrained GANs [5, 15–17] is previously exploited by GAN inversion [1, 11, 11], whose primary aim is to find the closest latent codes given an input image. Beyond GANs, Diffusion models have also been effectively used as generative priors in IR [18, 25, 43, 45], pushing the frontiers of advanced IR. Our work primarily focuses on generative priors derived from VAR [39], which has never been explored before.

3. Method

In this section, we provide a detailed introduction to our method. We first investigate the properties of VAR at different scales in Sec. 3.1. And then, we provide a detailed introduction to the structural design of VarFormer in Sec. 3.2.

3.1. Generative Priors in VAR for IR

Different from traditional autoregressive methods, VAR introduces a novel visual autoregressive modeling paradigm, shifting from "next-token prediction" to "next-scale prediction". This paradigm can solve mathematical inconsistencies and structural degradation, which is more optimal for generating highly-structured images. In VAR, each unit predicts an entire token map at a different scale. Starting with a 1×1 token map r_1 , VAR predicts a sequence of multi-scale token maps (r_1, r_2, \dots, r_K) , increasing in resolution. The generation process is expressed as:

$$p(r_1, r_2, \dots, r_K) = \prod_{k=1}^K p(r_k | r_1, r_2, \dots, r_{k-1}) \quad (1)$$

where $r_k \in [V]^{h_k \times w_k}$ represents the token map at scale k , with dimensions h_k and w_k , conditioned on previous maps $(r_1, r_2, \dots, r_{k-1})$. Each token in r_k is an index from the VQVAE codebook V , which is trained through multi-scale quantization and shared across scales.

To explore the information that VAR focuses on at different scales, we need it to model specific images. First, we obtain GT index sequence $F_e^{cle} = [F_{e_i}^{cle}]_{i=1}^N$ at various scales and provide them to VAR. To maintain the continuity and controllability of the VAR modeling process, we inject F_e^{cle} into the transformer using cross-attention. Finally, we decode the predicted sequence F_v^{cle} back to the pixel space. The pipeline is shown in Fig. 2. Please note that the reconstruction training process is conducted only on clean

images, with all modules except the cross-attention module being frozen. Following that, we replace the clean images with degraded images to obtain the GT index sequence $F_e^{deg} = [F_{e_i}^{deg}]_{i=1}^K$ and the sequence F_v^{deg} predicted by the Transformer. To explore the information that VAR focuses on at various scales, we replace the corresponding F_e^{deg} sequence with the specific scale sequence from F_v^{deg} . Then, we decode the new sequence back into the image space. The process can be mathematically formulated as:

$$I_{rec} = D\left(\sum_{i \notin C} F_{e_i}^{deg} + \sum_{i \in C} F_{v_i}^{deg}\right) \quad (2)$$

where D denotes the VAR Decoder, C refers to the set of indices that need to be replaced. In Fig. 2, it can be observed that VAR features at different scales naturally restore different types of typical degradation. Specifically, substituting lower scales can alleviate global degradations (e.g., low light and haze), while higher scales address local degradations (e.g., noise and rain). Furthermore, as shown in Fig. 3, by comparing the t-SNE diagrams of the latent representations F_e from the VQVAE encoder and F_v from the scale autoregression Transformer on various degraded images, the capability of VAR in effectively aligning distributions is demonstrated. Therefore, the reasonable combination of VAR features at different scales as priors can be beneficial to the image restoration process.

3.2. Architecture of the VarFormer

Based on the observations from Sec. 3.1, we propose VarFormer, which leverages the multi-scale distribution alignment priors in VAR to facilitate image restoration. As shown in Fig. 4, the VarFormer training process is divided into two stages. The first stage is dedicated to extracting the priors from VAR, while the second stage utilizes these priors to guide the restoration process. **In the first stage**, the model is enhanced with an Adapter module on top of the VAR that has been finetuned for reconstruction in Sec. 3.1. **In the second stage**, the model incorporates Degradation-Aware Enhancement (DAE) modules and Adaptive Feature Transformation (AFT) modules, which integrate the multi-scale distribution alignment priors extracted in the first phase to accomplish image restoration.

Adapter for Domain Shift (Train in Stage 1). Due to the existence of distributional shift between high quality sources for VAR pre-training and degraded datasets for image restoration, direct reuse of the features from the Encoder of VAR may be suboptimal. However, fine-tuning disrupts the the knowledge in VAR. Therefore, inspired by AWRCP [53], we chose to freeze the encoder and insert an Adapter containing self-attention blocks after it to retain pre-trained knowledge while narrowing the domain gap.

Degradation-Aware Enhancement (DAE) (Train in Stage 2). To address various degradation tasks by appropri-

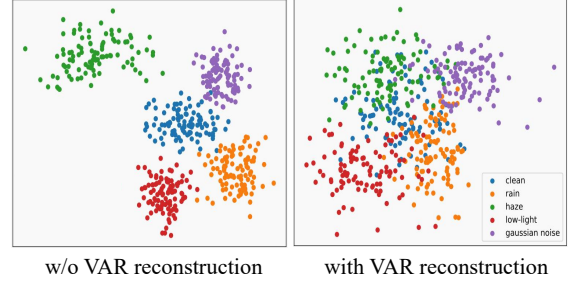


Figure 3. The t-SNE diagrams demonstrate that VAR’s next-scale prediction can reduce the gap between degraded and clean images, effectively aligning their distributions.

ately combining information at different scales, we propose Degradation-Aware Enhancement (DAE). An illustration of DAE is shown in Fig. 4. After reconstruction pre-training on extensive clean images, the encoder of VAR has developed the capability to discern what level of information each network layer should focus on. Consequently, we can use the outputs F_{e_v} from its different layers to determine the weights for scale priors. Specifically, for the i -th layer of the encoder or decoder in the second stage, we take $F_{e_v}^i$ as the input for the weight predictor within the DAE. After processing through Swin-transformer blocks that mitigate the impact of image content and a projection convolutional layer, we derive the weight prediction set $W = [w_i]_{i=1}^K$.

$$\widehat{S}_w^i = \mathcal{M}\left(\sum_{j=1}^K w_j \cdot S_v^j\right), \quad (3)$$

where the $\mathcal{M}(\cdot)$ is a lightweight projection head designed to perform dimensionality transformation on the re-weighted priors, the $\widehat{S}_w^i \in R^{C^i \times H^i \times W^i}$ is the re-weighted priors for i -th encoder or decoder layer.

Furthermore, we must consider that not every region in a degraded image may need to undergo the transition from the degraded domain to the clean domain. To adjust the guidance strength of the priors according to the degradation conditions of different regions, inspired by [28], we facilitate interaction between $F_{e/d}^i \in R^{C^i \times H^i \times W^i}$ and \widehat{S}_w^i at the channel level, enabling them to better capture long-range dependencies. After processing through a lightweight network, we obtain region-specific fusion weights w_1^g and w_2^g for $F_{e/d}^i$ and \widehat{S}_w^i , respectively. Ultimately, the feature $F_{g_{e/d}}^i \in R^{C^i \times H^i \times W^i}$ is derived by summing $F_{e/d}^i$ and \widehat{S}_w^i , each multiplied by their respective weights:

$$w_1^g, w_2^g = \text{Softmax}(\text{Conv}(\text{RSTBs}(\text{Concat}(F_{e/d}^i, \widehat{S}_w^i))))$$

$$F_{g_{e/d}}^i = F_{e/d}^i \times w_1^g + \widehat{S}_w^i \times w_2^g \quad (4)$$

where $\text{Concat}(\cdot)$ refers to the concatenation operation, the $\text{RSTBs}(\cdot)$ means a series of Residual Swin-Transformer

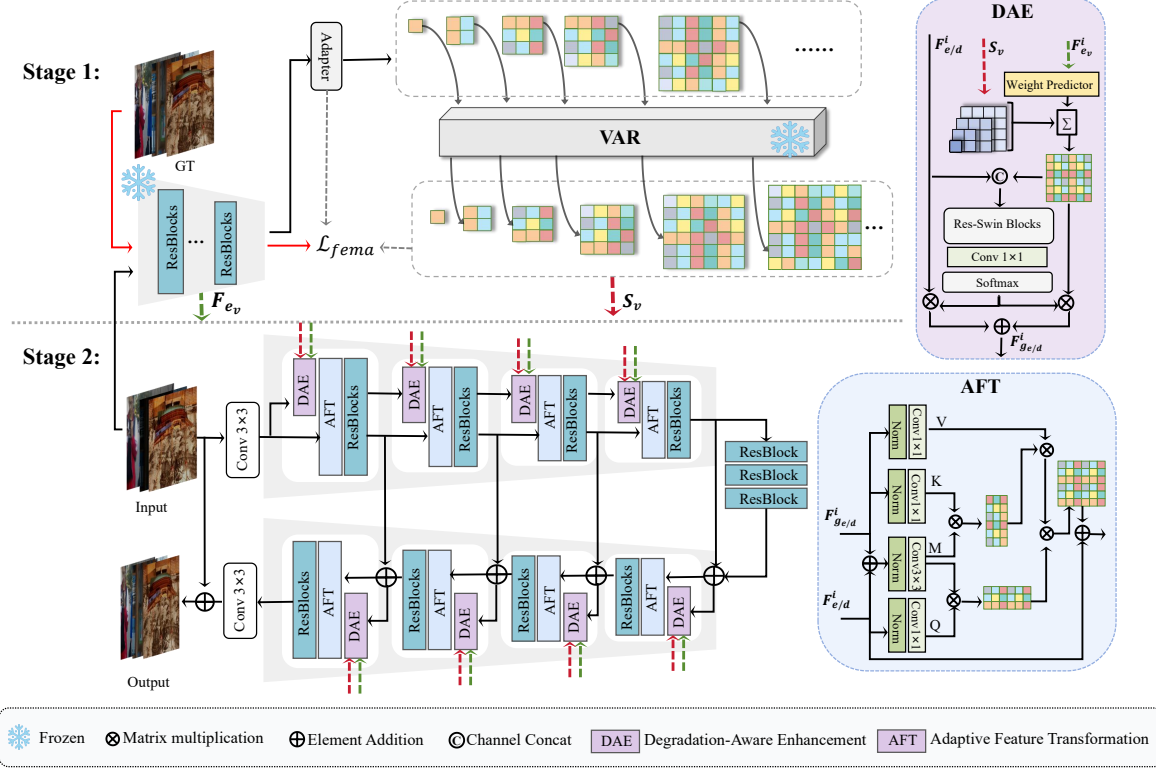


Figure 4. The framework of our VarFormer includes two training stages. **Stage 1:** To preserve the inherent knowledge of VAR and further enhance its adaptive distribution alignment capability, we freeze the VAR and integrate an Adapter to deliberately reduce the distance between the multi-scale latent representations of clean and degraded images, thereby obtaining multi-scale distribution alignment embedding S_v . **Stage 2:** To adaptively extract valuable VAR scale priors for input-specific degradation type, the Degradation-Aware Enhancement (DAE) module is designed to distinguish different degradation types and integrate relevant priors, thus providing effective scale-aware alignment prior for the restoration process. Furthermore, the Adaptive Feature Transformation (AFT) module integrates the VAR scale priors into the image restoration network to guide the elimination of degradation.

Blocks, the $Conv(\cdot)$ represents the convolutional layer and the $Softmax(\cdot)$ means the Softmax activation layer.

Adaptive Feature Transformation (AFT) (Train in Stage 2). We employ Adaptive Feature Transformation (AFT) to alleviate structural warping and textural distortion resulting from the fusion of high-quality priors and low-quality degraded features. Unlike standard cross-attention, we introduce a low-dimensional intermediate feature M that aggregates both $F_{g_e/d}^i$ and $F_{e/d}^i$ as the mediator for similarity comparison, as illustrated in Fig. 4. Specifically, given the intermediate feature $F_{e/d}^i$ and the degradation-aware enhanced feature $F_{g_e/d}^i$, we obtain the bridging feature $F_{m_e/d}^i = Concat(F_{g_e/d}^i, F_{e/d}^i)$, where $F_{m_e/d}^i \in R^{2C^i \times H^i \times W^i}$. Then, $F_{e/d}^i$ is projected into the query $Q = W_q F_{e/d}^i$, $F_{m_e/d}^i$ is projected into the mediator $M = W_m F_{m_e/d}^i$, and $F_{g_e/d}^i$ is projected into the key $K = W_k F_{g_e/d}^i$ and value $V = W_v F_{g_e/d}^i$. Here, W_m, W_q, W_k, W_v are all implemented using convolutional kernels.

Formally, the transformation process is defined by the following equations:

$$\begin{aligned} F_{in}^{i+1} &= A_{q,m} \cdot (A_{m,k} \cdot V) + F_{e/d}^i \\ A_{q,m} &= Softmax(Q \cdot M^T / \sqrt{d}) \\ A_{m,k} &= Softmax(M \cdot K^T / \sqrt{d}) \end{aligned} \quad (5)$$

where $L \ll H$, $A_{q,m} \in R^{H \times L}$ and $A_{m,k} \in R^{L \times H}$ denotes the attention map between the query-mediator pair and mediator-key pair.

In addition, to address the inherent loss of detail and texture due to downsampling operations, we propose an adaptive mix-up skipping to integrate encoder features into the decoder, thereby mitigating information loss:

$$F_d^i = \sigma(\theta_i) \times \hat{F}_d^i + (1 - \sigma(\theta_i)) \times F_e^i \quad (6)$$

where θ_i represents a learnable coefficient, σ denotes the sigmoid operator, and $\hat{F}_d^i \in R^{C^i \times H^i \times W^i}$ is the output of residual blocks of the i -th layer.

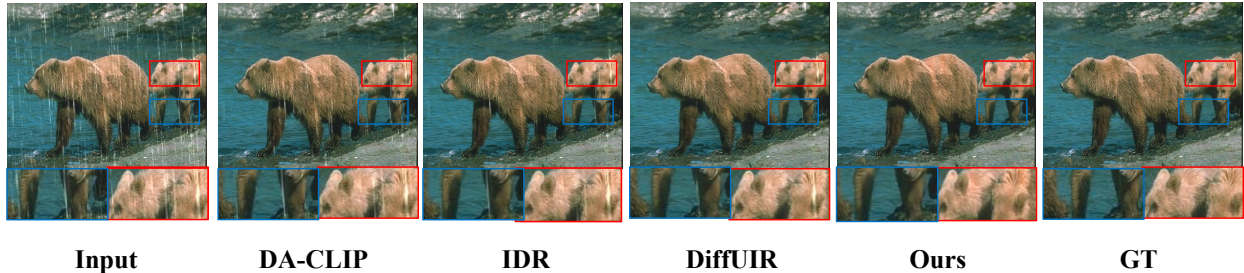


Figure 5. Visual comparison with state-of-the-art methods on image deraining task. Please zoom in for details.

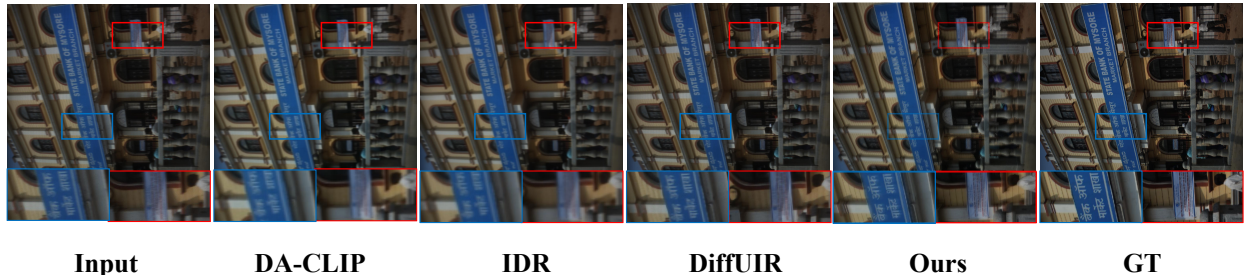


Figure 6. The visualization results of zero-shot generalization in real-world TOLED dataset. Please zoom in for details.

3.3. Training Objectives

Feature Matching Loss. The goal of the first stage is to further enhance the distribution alignment capability of VAR. Consequently, we design the Feature Matching Loss to reduce the feature discrepancies between degraded images and clean images, which can be formulated as follows:

$$\mathcal{L}_{fema} = \sum_{i=1}^K -s_i \log(\hat{s}_i) + \left\| F_a - sg(F_{e_{gt}}^q) \right\|_2^2 \quad (7)$$

where s_i is the ground-truth of i -th scale latent representation, \hat{s}_i is the output of VAR Transformer, and F_a is the output of Adapter.

Reconstruction Loss. This loss is utilized in the second training stage, with the purpose of ensuring that the restored image possesses a completed structure and impressing visual pleasure. It consists of two components: the PSNR loss and the perceptual loss. It is formulated as follows:

$$\mathcal{L}_{rec} = -PSNR(I_{gt}, I_{rec}) + \|\psi(I_{gt}) - \psi(I_{rec})\|_2^2 \quad (8)$$

where $\psi(\cdot)$ indicates the pre-trained VGG19 network.

4. Experiments

In this section, we first clarify the experimental settings of our method, and then present qualitative and quantitative results compared with the state-of-the-art methods on all-in-one and zero-shot tasks. Moreover, we also conduct extensive ablations to verify the effectiveness of our method.

4.1. Experimental Settings

Datasets. (1) All-in-one : We train a unified model to solve 6 IR tasks, including deraining, dehazing, low-light enhancement, motion deblurring, Gaussian denoising and real image denoising. For deraining, We adopt Rain13K [9, 22, 23, 29, 52] for training, and 5 datasets for testing, including Rain100L [51], Rain100H [51], Test100 [58], Test1200 [57] and Test2800 [10]. For dehazing, the RESIDE [20] dataset is used as the benchmark. As the real-world fog condition is outdoor, we only train and test on the outdoor part. For low-light enhancement, LOL dataset [48] is adopted. For motion deblurring, we adopt GoPro [35] dataset for training and testing. For Gaussian denoising, BSD400 [32] and WED [31] are used for training and BSD68 [33], Urban100 [14], Kodak24 [8] for testing. For real image denoising, We use SIDD [2] datasets as the benchmark for training and testing. (2) Zero-shot: we utilize TOLED [65] and POLED [65] for under-display camera (UDC) IR.

Evaluation Metrics. To evaluate the restoration performance, we adopt Signal to Noise Ratio (PSNR), Structural Similarity (SSIM) and Learned Perceptual Image Patch Similarity (LPIPS) [63]. We emphasize the performance of the universal methods, with the best results shown in **red**.

Implementation Details. We adopt the Adam optimizer [19] ($\beta_1 = 0.9$, $\beta_2 = 0.999$) with the initial learning rate $1e-4$ gradually reduced to $1e-6$ with cosine annealing to train our model. We random crop 256×256 patch from original image as network input after data augmentation.

Table 1. Quantitative comparison with state-of-the-art task-specific methods and universal methods on image deraining, low-light image enhancement, motion deblurring and image dehazing tasks.

Method	Year	Deraining (5sets)		Deblurring		Enhancement		Dehazing	
		PSNR \uparrow	SSIM \uparrow	PSNR \uparrow	SSIM \uparrow	PSNR \uparrow	SSIM \uparrow	PSNR \uparrow	SSIM \uparrow
Task-specific Method									
SwinIR [24]	2021	-	-	24.52	0.773	17.81	0.723	21.50	0.891
MIRNet [54]	2022	-	-	26.30	0.799	24.74	0.851	24.03	0.927
Restormer [56]	2022	33.96	0.935	32.92	0.961	20.41	0.806	30.87	0.969
MAXIM [41]	2022	33.24	0.933	32.86	0.940	23.43	0.863	-	-
RDDM [26]	2023	30.65	0.901	28.83	0.846	24.22	0.889	30.76	0.943
Universal Method									
AirNet [21]	2022	25.44	0.743	27.14	0.832	18.49	0.767	25.48	0.944
Painter [44]	2022	29.49	0.868	-	-	22.40	0.872	-	-
IDR [60]	2023	30.87	0.906	27.94	0.848	22.32	0.836	25.33	0.945
DA-CLIP [30]	2023	28.75	0.844	26.24	0.801	24.27	0.885	31.42	0.941
Prompt-IR [36]	2023	29.44	0.848	27.31	0.834	22.95	0.844	32.17	0.953
DiffUIR [64]	2024	31.14	0.907	29.88	0.874	25.02	0.901	32.74	0.944
VarFormer	-	31.33	0.913	30.99	0.956	25.13	0.917	32.96	0.956

Table 2. Quantitative results of Gaussian denoising on BSD68, Urban100 and Kodak24 datasets in terms of PSNR \uparrow .

Method	BSD68			Urban100			Kodak24		
	$\sigma=15$	$\sigma=25$	$\sigma=50$	$\sigma=15$	$\sigma=25$	$\sigma=50$	$\sigma=15$	$\sigma=25$	$\sigma=50$
HINet [6]	33.72	31.00	27.63	33.49	30.94	27.32	34.38	31.84	28.52
MPRNet [55]	34.01	31.35	28.08	34.13	31.75	28.41	34.77	32.31	29.11
MIRV2 [54]	33.66	30.97	27.66	33.30	30.75	27.22	34.29	31.81	28.55
SwinIR [24]	33.31	30.59	27.13	32.79	30.18	26.52	33.89	31.32	27.93
Restormer [56]	34.03	31.49	28.11	33.72	31.26	28.03	34.78	32.37	29.08
AirNet [21]	33.49	30.91	27.66	33.16	30.83	27.45	34.14	31.74	28.59
IDR [60]	34.05	31.67	28.05	32.92	31.29	28.45	34.53	32.22	28.93
DA-CLIP [30]	30.16	28.89	27.04	33.14	30.99	27.61	33.86	32.30	28.84
Prompt-IR [36]	32.17	29.89	28.03	33.04	31.89	27.72	33.78	32.21	28.64
DiffUIR [64]	33.86	30.88	26.63	32.19	29.65	25.87	33.24	30.70	27.19
VarFormer	34.11	31.85	28.23	33.13	31.94	28.96	34.73	32.40	29.02

As the data size varies greatly from task to task, we set the weight of each task in one batch as 0.3 for dehazing, 0.1 for low-light, 0.2 for deraining, 0.2 for Gaussian denoising, 0.1 for real image denoising, and 0.1 for motion deblurring.

4.2. All-in-One Restoration

We compare VarFormer with both task-specific and universal methods. To ensure a fair evaluation, we train all-in-one models from scratch using our training strategy. The quantitative results are presented in Tabs. 1 to 3, where it can be observed that VarFormer demonstrates superior performance across all 6 tasks. Notably, in low-light enhancement

Table 3. Quantitative results of Real image denoising on SIDD in terms of PSNR \uparrow and SSIM \uparrow .

Method	SIDD	
	PSNR \uparrow	SSIM \uparrow
MPRNet [55]	39.71	0.958
Uformer [46]	39.89	0.961
Restormer [56]	40.02	0.967
ART [59]	39.99	0.964
AirNet [21]	38.32	0.945
Prompt-IR [36]	39.52	0.954
DA-CLIP [30]	34.04	0.824
IDR [60]	39.74	0.957
MPerceiver [3]	39.96	0.959
Painter [44]	38.88	0.954
VarFormer	40.13	0.978

and dehazing tasks, VarFormer’s performance with the all-in-one training strategy even surpasses that of task-specific methods, highlighting its exceptional capabilities. We also provide visual comparisons with other state-of-the-art universal methods, as shown in Fig. 5, with more results available in the supplementary material. It is evident that, compared to other universal methods, VarFormer yields more steady results in all image restoration tasks.

4.3. Zero-shot Results

In Tab. 4, we present the generalization performance of various methods on unseen tasks without fine-tuning. Specifi-

cally, high-resolution images captured under under-display camera (UDC) systems often suffer from various types of degradations due to the point spread function and lower light transmission rate, posing challenges for the prediction of restoration models. Encouragingly, our VarFormer achieves state-of-the-art performance. For instance, as shown in Fig. 6, compared to other universal methods, our approach effectively addresses blurring.

Table 4. Quantitative results of unknown tasks (under-display camera image restoration) on TOLED and POLED datasets.

Method	TOLED			POLED		
	PSNR↑	SSIM↑	LPIPS↓	PSNR↑	SSIM↑	LPIPS↓
NAFNet [7]	26.89	0.774	0.346	10.83	0.416	0.794
HINet [6]	13.84	0.559	0.448	11.52	0.436	0.831
MPRNet [55]	24.69	0.707	0.347	8.34	0.365	0.798
DGUNet [34]	19.67	0.627	0.384	8.88	0.391	0.810
MIRV2 [54]	21.86	0.620	0.408	10.27	0.425	0.722
SwinIR [24]	17.72	0.661	0.419	6.89	0.301	0.852
Restormer [56]	20.98	0.632	0.360	9.04	0.399	0.742
TAPE [27]	17.61	0.583	0.520	7.90	0.219	0.799
AirNet [21]	14.58	0.609	0.445	7.53	0.350	0.820
DA-CLIP [30]	15.74	0.606	0.472	14.91	0.475	0.739
IDR [60]	27.91	0.795	0.312	16.71	0.497	0.716
DiffUIR [64]	29.55	0.866	0.281	15.62	0.424	0.505
VarFormer	30.61	0.887	0.275	16.63	0.499	0.605

4.4. Ablation Studies

In this section, we perform a series of ablation studies to better the effectiveness of our designs. In Tab. 5, we conduct ablation studies on the design of key components, including the adaptive mix-up skip that integrates encoder features into the decoder, the adapter that addresses the domain shift issue when using pre-trained VAR on degraded datasets, and the DAE and AFT modules responsible for generating and fusing multi-scale distribution alignment priors. We evaluate the performance based on the average performance across six tasks. The results indicate a gradual improvement with the addition of each component and a corresponding decline when each component is removed, underscoring the effectiveness of each module.

Additionally, we explored the influence of the guidance strength of VAR multi-scale priors on restoration tasks by altering the quantity of DAE modules. The results from Tab. 6 indicate a positive correlation between model performance and the guidance strength provided by VAR priors. This discovery indicates that the multi-scale priors within VAR exhibit notable effectiveness in directing the optimization trajectory of intricate multi-task restoration endeavors, effectively steering the model towards enhancing perfor-

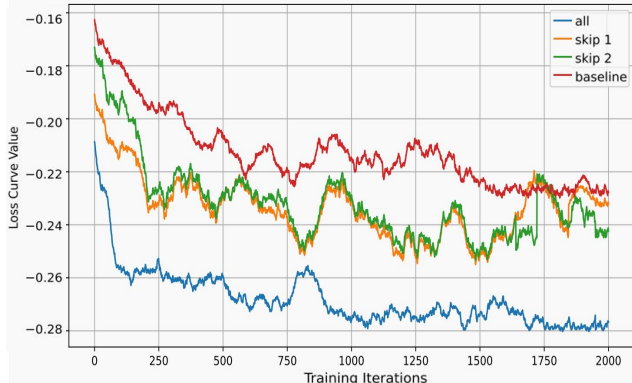


Figure 7. The training trajectory using different number of DAE.

Table 5. Ablation experiments on the components design.

Exp.	skip	adapter	AFT	DAE	PSNR↑	SSIM↑
a					27.54	0.841
b		✓	✓	✓	29.37	0.905
c	✓		✓	✓	29.51	0.917
d	✓	✓		✓	29.29	0.891
e	✓		✓		28.98	0.867
f	✓	✓	✓	✓	29.66	0.926

Table 6. Ablation experiments on the DAE number.

Exp.	DAE				PSNR↑	SSIM↑
	all	skip1	skip2	w/o		
a				✓	28.98	0.867
b			✓		29.29	0.883
c		✓			29.49	0.902
d	✓				29.66	0.926

mance. The training trajectories illustrated in Fig. 7 also support this conclusion, indicating that the integration of DAE modules can accelerate the model’s convergence.

5. Conclusion

In this paper, we investigate the multi-scale representations of the generative model VAR and reveal its endogenous multi-scale priors. As the autoregressive scales evolve, it transitions from capturing global color information to focusing on fine-grained details and adaptively aligns the input with clean images scale by scale. Furthermore, we propose the VarFormer framework integrated with multi-scale priors for multiple degradation restoration. Extensive experiments on various image restoration tasks demonstrate the effectiveness and generalization of our method.

References

- [1] Rameen Abdal, Yipeng Qin, and Peter Wonka. Image2stylegan: How to embed images into the stylegan latent space? In *Proceedings of the IEEE/CVF international conference on computer vision*, pages 4432–4441, 2019. 3
- [2] Abdelrahman Abdelhamed, Stephen Lin, and Michael S Brown. A high-quality denoising dataset for smartphone cameras. In *Proceedings of the IEEE conference on computer vision and pattern recognition*, pages 1692–1700, 2018. 6
- [3] Yuang Ai, Huaibo Huang, Xiaoqiang Zhou, Jiexiang Wang, and Ran He. Multimodal prompt perceiver: Empower adaptiveness generalizability and fidelity for all-in-one image restoration. In *Proceedings of the IEEE/CVF Conference on Computer Vision and Pattern Recognition*, pages 25432–25444, 2024. 7
- [4] S. Derin Babacan, Rafael Molina, and Aggelos K. Katsaggelos. Variational bayesian blind deconvolution using a total variation prior. *IEEE Transactions on Image Processing*, 18: 12–26, 2009. 3
- [5] Andrew Brock. Large scale gan training for high fidelity natural image synthesis. *arXiv preprint arXiv:1809.11096*, 2018. 3
- [6] Liangyu Chen, Xin Lu, Jie Zhang, Xiaojie Chu, and Chengpeng Chen. Hinet: Half instance normalization network for image restoration. In *Proceedings of the IEEE/CVF conference on computer vision and pattern recognition*, pages 182–192, 2021. 7, 8
- [7] Liangyu Chen, Xiaojie Chu, Xiangyu Zhang, and Jian Sun. Simple baselines for image restoration. In *European conference on computer vision*, pages 17–33. Springer, 2022. 8
- [8] Rich Franzen. Kodak lossless true color image suite. <http://r0k.us/graphics/kodak>, 1999. Accessed: 1999-06-07. 6
- [9] Xueyang Fu, Jiabin Huang, Xinghao Ding, Yinghao Liao, and John William Paisley. Clearing the skies: A deep network architecture for single-image rain removal. *IEEE Transactions on Image Processing*, 26:2944–2956, 2016. 6
- [10] Xueyang Fu, Jiabin Huang, Delu Zeng, Yue Huang, Xinghao Ding, and John William Paisley. Removing rain from single images via a deep detail network. *2017 IEEE Conference on Computer Vision and Pattern Recognition (CVPR)*, pages 1715–1723, 2017. 6
- [11] Jinjin Gu, Yujun Shen, and Bolei Zhou. Image processing using multi-code gan prior. In *Proceedings of the IEEE/CVF conference on computer vision and pattern recognition*, pages 3012–3021, 2020. 3
- [12] Chunle Guo, Chongyi Li, Jichang Guo, Chen Change Loy, Junhui Hou, Sam Kwong, and Runmin Cong. Zero-reference deep curve estimation for low-light image enhancement. In *Proceedings of the IEEE/CVF conference on computer vision and pattern recognition*, pages 1780–1789, 2020. 1
- [13] Kaiming He, Jian Sun, and Xiaoou Tang. Single image haze removal using dark channel prior. *IEEE transactions on pattern analysis and machine intelligence*, 33(12):2341–2353, 2010. 3
- [14] Jia-Bin Huang, Abhishek Singh, and Narendra Ahuja. Single image super-resolution from transformed self-exemplars. *2015 IEEE Conference on Computer Vision and Pattern Recognition (CVPR)*, pages 5197–5206, 2015. 6
- [15] Tero Karras. Progressive growing of gans for improved quality, stability, and variation. *arXiv preprint arXiv:1710.10196*, 2017. 3
- [16] Tero Karras, Samuli Laine, and Timo Aila. A style-based generator architecture for generative adversarial networks. In *Proceedings of the IEEE/CVF conference on computer vision and pattern recognition*, pages 4401–4410, 2019.
- [17] Tero Karras, Samuli Laine, Miika Aittala, Janne Hellsten, Jaakko Lehtinen, and Timo Aila. Analyzing and improving the image quality of stylegan. In *Proceedings of the IEEE/CVF conference on computer vision and pattern recognition*, pages 8110–8119, 2020. 3
- [18] Bahjat Kawar, Michael Elad, Stefano Ermon, and Jiaming Song. Denoising diffusion restoration models. *Advances in Neural Information Processing Systems*, 35:23593–23606, 2022. 2, 3
- [19] Diederik P. Kingma and Jimmy Ba. Adam: A method for stochastic optimization. *arXiv preprint arXiv:1412.6980*, 2014. 6
- [20] Boyi Li, Wenqi Ren, Dengpan Fu, Dacheng Tao, Dan Feng, Wenjun Zeng, and Zhangyang Wang. Benchmarking single-image dehazing and beyond. *IEEE Transactions on Image Processing*, 28(1):492–505, 2018. 6
- [21] Boyun Li, Xiao Liu, Peng Hu, Zhongqin Wu, Jiancheng Lv, and Xiaocui Peng. All-in-one image restoration for unknown corruption. *2022 IEEE/CVF Conference on Computer Vision and Pattern Recognition (CVPR)*, pages 17431–17441, 2022. 1, 7, 8
- [22] Xia Li, Jianlong Wu, Zhouchen Lin, Hong Liu, and Hongbin Zha. Recurrent squeeze-and-excitation context aggregation net for single image deraining. *ArXiv*, abs/1807.05698, 2018. 6
- [23] Yu Li, Robby T. Tan, Xiaojie Guo, Jiangbo Lu, and M. S. Brown. Rain streak removal using layer priors. *2016 IEEE Conference on Computer Vision and Pattern Recognition (CVPR)*, pages 2736–2744, 2016. 6
- [24] Jingyun Liang, Jiezhong Cao, Guolei Sun, Kai Zhang, Luc Van Gool, and Radu Timofte. Swinir: Image restoration using swin transformer. In *Proceedings of the IEEE/CVF international conference on computer vision*, pages 1833–1844, 2021. 7, 8
- [25] Xinqi Lin, Jingwen He, Ziyang Chen, Zhaoyang Lyu, Bo Dai, Fanghua Yu, Wanli Ouyang, Yu Qiao, and Chao Dong. Diffbir: Towards blind image restoration with generative diffusion prior. *arXiv preprint arXiv:2308.15070*, 2023. 2, 3
- [26] Jiawei Liu, Qiang Wang, Huijie Fan, Yinong Wang, Yandong Tang, and Liangqiong Qu. Residual denoising diffusion models. In *Proceedings of the IEEE/CVF Conference on Computer Vision and Pattern Recognition*, pages 2773–2783, 2024. 7
- [27] Lin Liu, Lingxi Xie, Xiaopeng Zhang, Shanxin Yuan, Xiangyu Chen, Wengang Zhou, Houqiang Li, and Qi Tian. Tape: Task-agnostic prior embedding for image restoration.

- In *European Conference on Computer Vision*, pages 447–464. Springer, 2022. 8
- [28] Yi Liu, Jiachen Li, Yanchun Ma, Qing Xie, and Yongjian Liu. Hcanet: Haze-concentration-aware network for real-scene dehazing with codebook priors. In *Proceedings of the 32nd ACM International Conference on Multimedia*, pages 9136–9144, 2024. 4
- [29] Yu Luo, Yong Xu, and Hui Ji. Removing rain from a single image via discriminative sparse coding. *2015 IEEE International Conference on Computer Vision (ICCV)*, pages 3397–3405, 2015. 6
- [30] Ziwei Luo, Fredrik K Gustafsson, Zheng Zhao, Jens Sjölund, and Thomas B Schön. Controlling vision-language models for universal image restoration. *arXiv preprint arXiv:2310.01018*, 3(8), 2023. 7, 8
- [31] Kede Ma, Zhengfang Duanmu, Qingbo Wu, Zhou Wang, Hongwei Yong, Hongliang Li, and Lei Zhang. Waterloo exploration database: New challenges for image quality assessment models. *IEEE Transactions on Image Processing*, 26(2):1004–1016, 2016. 6
- [32] David Martin, Charless Fowlkes, Doron Tal, and Jitendra Malik. A database of human segmented natural images and its application to evaluating segmentation algorithms and measuring ecological statistics. In *Proceedings eighth IEEE international conference on computer vision. ICCV 2001*, pages 416–423. IEEE, 2001. 6
- [33] David R. Martin, Charless C. Fowlkes, Doron Tal, and Jitendra Malik. A database of human segmented natural images and its application to evaluating segmentation algorithms and measuring ecological statistics. *Proceedings Eighth IEEE International Conference on Computer Vision. ICCV 2001*, 2: 416–423 vol.2, 2001. 6
- [34] Chong Mou, Qian Wang, and Jian Zhang. Deep generalized unfolding networks for image restoration. In *Proceedings of the IEEE/CVF conference on computer vision and pattern recognition*, pages 17399–17410, 2022. 3, 8
- [35] Seungjun Nah, Tae Hyun Kim, and Kyoung Mu Lee. Deep multi-scale convolutional neural network for dynamic scene deblurring. *2017 IEEE Conference on Computer Vision and Pattern Recognition (CVPR)*, pages 257–265, 2016. 6
- [36] V Potlapalli, SW Zamir, S Khan, and FS Khan. Promptir: Prompting for all-in-one blind image restoration. *arXiv 2023. arXiv preprint arXiv:2306.13090*. 7
- [37] Yuhui Quan, Zicong Wu, and Hui Ji. Neumann network with recursive kernels for single image defocus deblurring. In *Proceedings of the IEEE/CVF Conference on Computer Vision and Pattern Recognition*, pages 5754–5763, 2023. 1
- [38] Lingyan Ruan, Bin Chen, Jizhou Li, and Miuling Lam. Learning to deblur using light field generated and real defocus images. In *Proceedings of the IEEE/CVF Conference on Computer Vision and Pattern Recognition*, pages 16304–16313, 2022. 1
- [39] Keyu Tian, Yi Jiang, Zehuan Yuan, Bingyue Peng, and Liwei Wang. Visual autoregressive modeling: Scalable image generation via next-scale prediction. *arXiv preprint arXiv:2404.02905*, 2024. 2, 3
- [40] Fu-Jen Tsai, Yan-Tsung Peng, Yen-Yu Lin, Chung-Chi Tsai, and Chia-Wen Lin. Stripformer: Strip transformer for fast image deblurring. In *European conference on computer vision*, pages 146–162. Springer, 2022. 1
- [41] Zhengzhong Tu, Hossein Talebi, Han Zhang, Feng Yang, Peyman Milanfar, Alan Bovik, and Yinxiao Li. Maxim: Multi-axis mlp for image processing. In *Proceedings of the IEEE/CVF conference on computer vision and pattern recognition*, pages 5769–5780, 2022. 7
- [42] Jeya Maria Jose Valanarasu, Rajeev Yasarla, and Vishal M Patel. Transweather: Transformer-based restoration of images degraded by adverse weather conditions. In *Proceedings of the IEEE/CVF Conference on Computer Vision and Pattern Recognition*, pages 2353–2363, 2022. 3
- [43] Jianyi Wang, Zongsheng Yue, Shangchen Zhou, Kelvin CK Chan, and Chen Change Loy. Exploiting diffusion prior for real-world image super-resolution. *International Journal of Computer Vision*, pages 1–21, 2024. 3
- [44] Xinlong Wang, Wen Wang, Yue Cao, Chunhua Shen, and Tiejun Huang. Images speak in images: A generalist painter for in-context visual learning. In *Proceedings of the IEEE/CVF Conference on Computer Vision and Pattern Recognition*, pages 6830–6839, 2023. 7
- [45] Yinhuai Wang, Jiwen Yu, and Jian Zhang. Zero-shot image restoration using denoising diffusion null-space model. *arXiv preprint arXiv:2212.00490*, 2022. 2, 3
- [46] Zhendong Wang, Xiaodong Cun, Jianmin Bao, and Jianzhuang Liu. Uformer: A general u-shaped transformer for image restoration. *2022 IEEE/CVF Conference on Computer Vision and Pattern Recognition (CVPR)*, pages 17662–17672, 2021. 7
- [47] Zichun Wang, Ying Fu, Ji Liu, and Yulun Zhang. Lg-bpn: Local and global blind-patch network for self-supervised real-world denoising. In *Proceedings of the IEEE/CVF Conference on Computer Vision and Pattern Recognition*, pages 18156–18165, 2023. 1
- [48] Chen Wei, Wenjing Wang, Wenhan Yang, and Jiaying Liu. Deep retinex decomposition for low-light enhancement. *ArXiv*, abs/1808.04560, 2018. 6
- [49] Yuhui Wu, Chen Pan, Guoqing Wang, Yang Yang, Jiwei Wei, Chongyi Li, and Heng Tao Shen. Learning semantic-aware knowledge guidance for low-light image enhancement. In *Proceedings of the IEEE/CVF Conference on Computer Vision and Pattern Recognition*, pages 1662–1671, 2023. 1
- [50] Xiaogang Xu, Ruixing Wang, and Jiangbo Lu. Low-light image enhancement via structure modeling and guidance. In *Proceedings of the IEEE/CVF Conference on Computer Vision and Pattern Recognition*, pages 9893–9903, 2023. 1
- [51] Wenhan Yang, Robby T. Tan, Jiashi Feng, Jiaying Liu, Zongming Guo, and Shuicheng Yan. Deep joint rain detection and removal from a single image. *2017 IEEE Conference on Computer Vision and Pattern Recognition (CVPR)*, pages 1685–1694, 2016. 6
- [52] Wenhan Yang, Robby T. Tan, Shiqi Wang, Yuming Fang, and Jiaying Liu. Single image deraining: From model-based to data-driven and beyond. *IEEE Transactions on Pattern Analysis and Machine Intelligence*, 43:4059–4077, 2019. 6
- [53] Tian Ye, Sixiang Chen, Jinbin Bai, Jun Shi, Chenghao Xue, Jingxia Jiang, Junjie Yin, Erkang Chen, and Yun Liu. Adverse weather removal with codebook priors. In *Proceedings*

- of the *IEEE/CVF International Conference on Computer Vision*, pages 12653–12664, 2023. 4
- [54] Syed Waqas Zamir, Aditya Arora, Salman Khan, Munawar Hayat, Fahad Shahbaz Khan, Ming-Hsuan Yang, and Ling Shao. Learning enriched features for real image restoration and enhancement. In *Computer Vision–ECCV 2020: 16th European Conference, Glasgow, UK, August 23–28, 2020, Proceedings, Part XXV 16*, pages 492–511. Springer, 2020. 7, 8
- [55] Syed Waqas Zamir, Aditya Arora, Salman Hameed Khan, Munawar Hayat, Fahad Shahbaz Khan, Ming-Hsuan Yang, and Ling Shao. Multi-stage progressive image restoration. *2021 IEEE/CVF Conference on Computer Vision and Pattern Recognition (CVPR)*, pages 14816–14826, 2021. 1, 7, 8
- [56] Syed Waqas Zamir, Aditya Arora, Salman Khan, Munawar Hayat, Fahad Shahbaz Khan, and Ming-Hsuan Yang. Restormer: Efficient transformer for high-resolution image restoration. In *Proceedings of the IEEE/CVF conference on computer vision and pattern recognition*, pages 5728–5739, 2022. 7, 8
- [57] He Zhang and Vishal M. Patel. Density-aware single image de-raining using a multi-stream dense network. *2018 IEEE/CVF Conference on Computer Vision and Pattern Recognition*, pages 695–704, 2018. 6
- [58] He Zhang, Vishwanath A. Sindagi, and Vishal M. Patel. Image de-raining using a conditional generative adversarial network. *IEEE Transactions on Circuits and Systems for Video Technology*, 30:3943–3956, 2017. 6
- [59] Jiale Zhang, Yulun Zhang, Jinjin Gu, Yongbing Zhang, Linghe Kong, and Xin Yuan. Accurate image restoration with attention retractable transformer. *arXiv preprint arXiv:2210.01427*, 2022. 7
- [60] Jinghao Zhang, Jie Huang, Mingde Yao, Zizheng Yang, Hu Yu, Man Zhou, and Feng Zhao. Ingredient-oriented multi-degradation learning for image restoration. In *Proceedings of the IEEE/CVF Conference on Computer Vision and Pattern Recognition*, pages 5825–5835, 2023. 1, 3, 7, 8
- [61] Kai Zhang, Wangmeng Zuo, Yunjin Chen, Deyu Meng, and Lei Zhang. Beyond a gaussian denoiser: Residual learning of deep cnn for image denoising. *IEEE transactions on image processing*, 26(7):3142–3155, 2017. 1
- [62] Kai Zhang, Yawei Li, Jingyun Liang, Jie Zhang Cao, Yulun Zhang, Hao Tang, Radu Timofte, and Luc Van Gool. Practical blind denoising via swin-conv-unet and data synthesis. *arXiv e-prints*, pages arXiv–2203, 2022. 1
- [63] Richard Zhang, Phillip Isola, Alexei A Efros, Eli Shechtman, and Oliver Wang. The unreasonable effectiveness of deep features as a perceptual metric. In *Proceedings of the IEEE conference on computer vision and pattern recognition*, pages 586–595, 2018. 6
- [64] Dian Zheng, Xiao-Ming Wu, Shuzhou Yang, Jian Zhang, Jian-Fang Hu, and Wei-Shi Zheng. Selective hourglass mapping for universal image restoration based on diffusion model. In *Proceedings of the IEEE/CVF Conference on Computer Vision and Pattern Recognition*, pages 25445–25455, 2024. 7, 8
- [65] Yuqian Zhou, David Ren, Neil Emerton, Sehoon Lim, and Timothy Large. Image restoration for under-display camera. In *Proceedings of the IEEE/CVF conference on computer vision and pattern recognition*, pages 9179–9188, 2021. 6